Università degli Studi di Napoli "Federico II"

SCUOLA POLITECNICA E DELLE SCIENZE DI BASE

DIPARTIMENTO DI INGEGNERIA INDUSTRIALE

CORSO DI LAUREA IN INGEGNERIA AEROSPAZIALE

CLASSE DELLE LAUREE IN INGEGNERIA INDUSTRIALE (L-9)

Elaborato di laurea in Meccanica del Volo

Avanced modelling in OpenVSP to evaluate the stability and control characteristics of a 19-pax aircraft model with distributed propulsion

Relatore:
Prof. Danilo Ciliberti

Candidato:
Federica Marino
Matr. N35003453

ANNO ACCADEMICO 2023 – 2024

Dedication page

Abstract

The aim of this work is the evaluation of the propulsive effects on the stability and control of an innovative 19-seater aircraft model with distributed propulsion. The objective is achieved with the use of OpenVSP, an open-source tool developed by NASA, and its companion numerical aerodynamic solver VSPAERO. The first software allows to create a 3D model of the aircraft. The second is a vortex lattice solver, which uses OpenVSP geometries to evaluate the aerodynamics of the aircraft subject to different flow conditions. In particular, OpenVSP was used to create the 3D model of the propellers for both thermal and electric engines. Subsequently, the results obtained have been compared with those obtained with the use of the actuator disk model. Results have shown that for the calculation of the propulsive effects with the rotating propeller model, if this converges well, it leads to results very similar to those with the actuator disk.

Sommario

Lo scopo di questo lavoro è la valutazione degli effetti propulsivi sulla stabilità e sul controllo di un innovativo modello di aereo da 19 posti a propulsione distribuita. L'obiettivo è raggiunto con l'uso di OpenVSP, uno strumento open source sviluppato dalla NASA, e del suo solutore aerodinamico numerico VSPAERO. Il primo software consente di creare un modello 3D dell'aereo. Il secondo è un risolutore di reticoli di vortici, che utilizza le geometrie OpenVSP per valutare l'aerodinamica dell'aereo soggetto a diverse condizioni di flusso. In particolare, OpenVSP è stato utilizzato per realizzare il modello 3D delle eliche sia per motori termici che elettrici. Successivamente i risultati ottenuti sono stati confrontati con quelli ottenuti con l'utilizzo del modello a disco attuatore. I risultati hanno dimostrato che per il calcolo degli effetti propulsivi con il modello di elica rotante, se questa converge bene, porta ad avere risultati molto simili a quelli con il disco attuatore.

Table of contents

List of figures

List of tables

1. Introduction

1.1 Objective

The aim of this thesis is the evaluation of the propulsive effects on the stability and control of an innovative 19-pax aircraft with distributed propulsion. First of all, the two types of propellers, thermal and electric, were created with the OpenVSP geometric modeller, then they were positioned along the semi-wings of the aircraft, for a total of 8 propellers driven by electric motors and 2 propellers driven by thermal engines. Following several tests carried out to try to resolve the onset of some aerodynamic and data processing problems, the geometric model of the starting aircraft was modified by first considering the isolated electric propeller and subsequently coupled to the wing and horizontal tail plane. An analysis was then performed to evaluate the performance of the model with the vortex lattice solver, VSPAERO. The results collected on the aerodynamic forces and moments acting on the aircraft were plotted on spreadsheets and compared with those obtained with the actuator disk. By doing so it was possible to evaluate the effect of the rotating propellers compared to the classic simplification used up to now.

1.2 Layout of work

Chapter 2: This chapter is about theoretical principles and methods which this thesis project is based on.

Chapter 3: This chapter introduces the geometric model of rotating propellers, OpenVSP and VSPAERO setup.

Chapter 4: This chapter shows the data collected from the analyzes and the related comparative graphs.

Chapter 5: Conclusion chapter.

2. Theoretical overview

2.1 DEP principle

The concept behind Distributed Electric Propulsion (DEP) technology is to use multiple electric thrusters with the aim of producing a beneficial aerodynamic-propulsion interaction. The propellers used for this principle include two different types of DEP: small, high-lift propellers distributed along the leading edge to accelerate the flow over a wing at low speed, and larger cruise propellers placed together at each end wing to provide primary propulsive power. High-lift propellers allow for a high-load wing that is more efficient in cruising without sacrificing low-speed performance, while wingtip cruising propellers allow for increased propulsive efficiency, as well as reduction in drag induced through interactions between the wingtip thrusters and the wing drag vortex system [2].

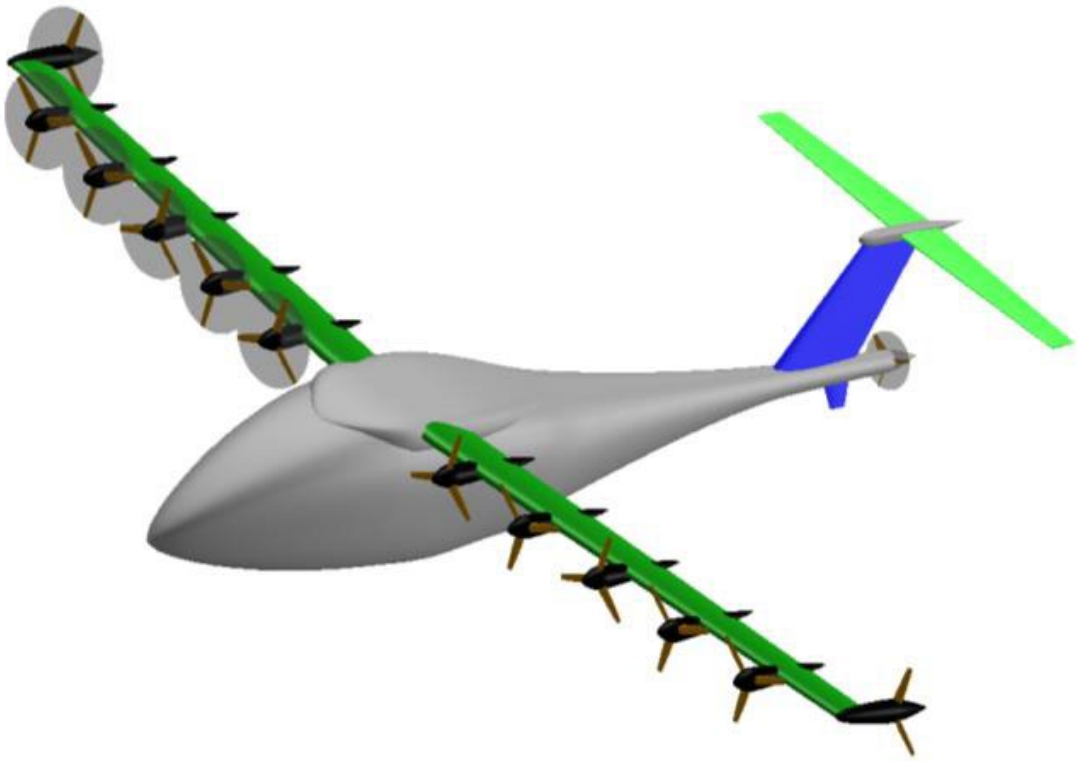

Figure 2.1: Implementation of distributed electric propulsion technology.

Being able to increase the dynamic pressure on the wing at low speed enables the advantage of using a smaller wing so as to have greater cruising efficiency at high speed without compromising low-speed performance, as it is necessary for take-off and landing [1]. A further advantage of DEP technology compared to more traditional designs is that of being able to position, size and use the thrusters with greater flexibility, making the most of the advantages of the aero-propulsive coupling and providing improved performance. Increasing the effective bypass ratio of the propulsion system can enable reduction of ambient noise during takeoff and landing and greater propulsive efficiency in all flight conditions [2]. Further research has focused on the design of high-lift propellers by attempting to maintain a nearly uniform axial velocity profile in the wake of the propeller to maximize the increase in lift. To produce blades that have these nearly uniform velocity profiles, different blade shapes are required than traditional Minimum Induced Loss (MIL) propellers. The propeller design method is based on longer chord lengths and twists near the root and reduced chord lengths and twists near the center of the blade [3].

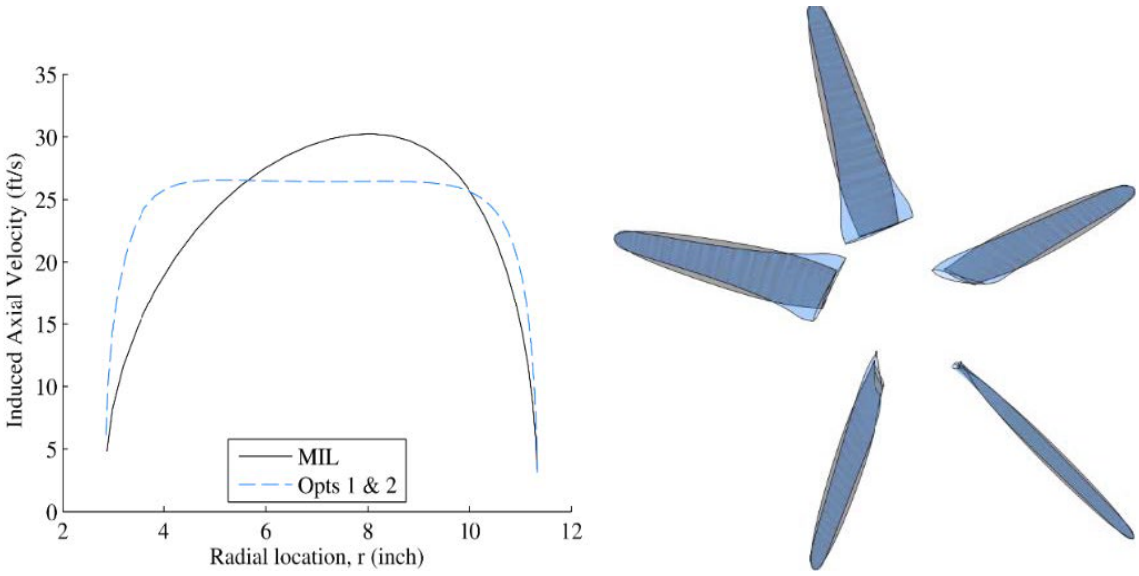

Figure 2.2: Comparison between high-lift propeller designs and their MIL counterparts.

Before achieving widespread production, there are several challenges to address, which include structural robustness, noise abatement strategies and the low specific energy of current battery technologies [2].

2.2 Actuator Disk Theory

The actuator disk theory is also called momentum theory and is based on the application of the laws of conservation of fluid mechanics to the rotor and flows. The theory behind the actuator disk assumes that:

- the propeller is replaced by an actuator disc;
- the actuator disk is often idealized as a thin, flat disk, with projected frontal area A;
- it is assumed that the fluid is incompressible and non-viscous, which means that there is no frictional resistance between the fluid layers;
- the propeller is characterized by a pressure jump that accelerates the air through the disc;
- the analysis often assumes steady-state flow conditions, where the flow properties do not change, simplifying the mathematical formulation;
- static pressures far from the disk are assumed to be equal to atmospheric pressure;
- the actuator disc provides a gradual change in flow speed, accelerating it downstream [4].

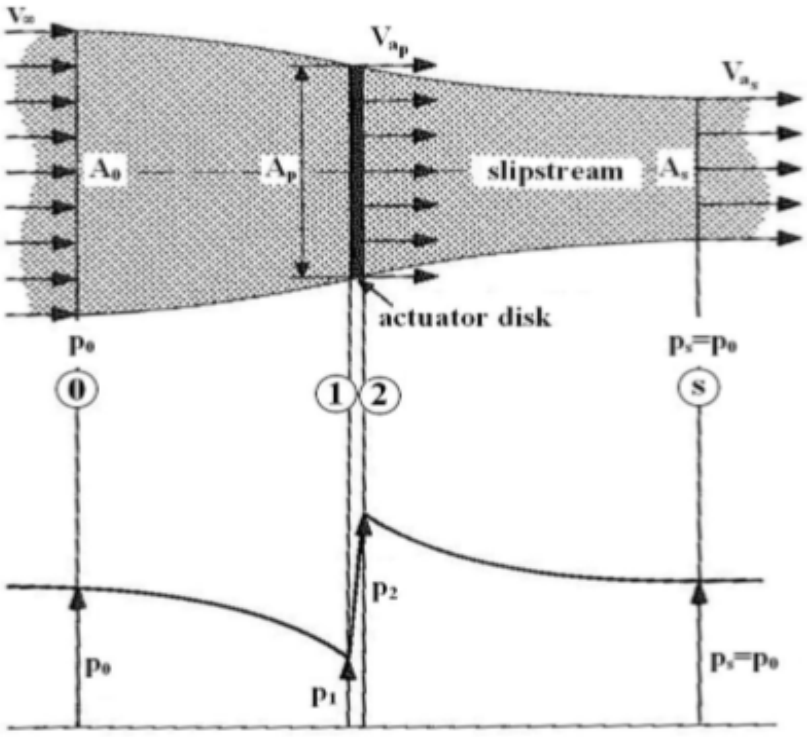

Figure 2.3: Velocity and static pressure distribution due to momentum theory.

The thrust of the propeller is:

$$T = \rho V_{as} A_s (V_{as} - V_\infty) \tag{2.1}$$

where V_{as} is the velocity far downstream, where the pressure has returned to the ambient value while area A is the cross-sectional area of the wake. The thrust is also equal to the pressure variation across the disk:

$$T = A_p (p_2 - p_1) = A_p \Delta_p \tag{2.2}$$

where A_p is the area of the propeller disc. The application of the Bernoulli equation upstream of the disk leads to the following equation:

$$p_0 + \frac{1}{2}\rho {V_\infty}^2 = p_1 + \frac{1}{2}\rho V_{Ap}^2 \tag{2.3}$$

While downstream:

$$p_2 + \frac{1}{2}\rho V_{ap}^2 = p_0 + \frac{1}{2}\rho V_{as}^2 \tag{2.4}$$

Subtracting the last two equations gives the pressure jump:

$$\Delta_p = \frac{1}{2}(V_{as}^2 - V_\infty^2) \tag{2.5}$$

Substituting the latter in (2.2) we obtain:

$$T = \frac{1}{2}\rho A_p (V_{ap}^2 - V_\infty^2) \tag{2.6}$$

The continuity equation is:

$$V_{ap} A_p = V_{as} A_s \tag{2.7}$$

Combining equation (2.1), (2.6) e (2.7) we obtain:

$$V_{ap} = \frac{1}{2}(V_\infty + V_{as}) \tag{2.8}$$

The last equation states that the axial velocity on the actuator disk is the arithmetic mean between the free stream axial velocity V_∞ and the flow axial velocity V_{as}. The power of the propeller is given by the product between the thrust (2.6) and the speed of the actuator disk (2.8):

$$P = \frac{1}{2}\rho A_p V_{ap}(V_{as}^2 - V_\infty^2) \tag{2.9}$$

It can be shown that the propulsive efficiency is equal to:

$$\eta = \frac{TV_\infty}{P} = \frac{2V_\infty}{V_{as}+V_\infty} \tag{2.10}$$

Substituting (2.8) into (2.10) we have:

$$\eta = \frac{V_\infty}{V_{ap}} \tag{2.11}$$

One of the limitations of the actuator disk theory is that it does not consider the design of the propeller blades. Consequently, if at the design stage it is necessary to know the details of the design of the individual propeller blades, then the actuator disk theory is inadequate [5].

2.3 Vortex Lattice Method (VLM)

The vortex lattice method (VLM) is a numerical method used primarily in computational fluid dynamics in the early stages of aircraft design to model lifting surfaces or parts thereof. By simulating the flow field, it is possible to extract the distribution of aerodynamic forces around the aircraft and evaluate its handling qualities at a conceptual level at the design stage [5]. This method is based on the application of some assumptions, such as:

- the flow field is incompressible, inviscid and irrotational;
- the lifting surfaces are considered thin, neglecting the effects of thickness on the aerodynamic surfaces;
- the small angle approximation is used, i.e. both the attack angle and the side slip angle are considered small [4].

The vortex lattice method approximates the surface into a mean surface, and then divides it into flat quadrilaterals. Each vortex generated by the quadrilateral satisfies boundary conditions based on the Kutta condition.

Starting from the irrotational flow we have:

$$\nabla \times V = 0 \tag{2.12}$$

and considering a potential Φ we obtain:

$$\nabla \times (\nabla \Phi) = 0 \tag{2.13}$$

The combination of equations (2.12) and (2.13) leads to:

$$V = \nabla \Phi \tag{2.14}$$

Equation (2.14) represents irrotational and incompressible flow. Since the continuity equation turns out to be valid, it is possible to consider the following equation:

$$\nabla \cdot V = 0 \tag{2.15}$$

From the union of equations (2.14) and (2.15) we have:

$$\nabla \cdot (\nabla \Phi) = 0 \tag{2.16}$$

or in another form:

$$\nabla^2 \Phi = 0 \tag{2.17}$$

The latter is the Laplace equation which allows any irrotational and incompressible flow to be described as the combination of a series of elementary irrotational and incompressible flows. The problem can be easily solved by applying the following boundary conditions to the Laplace equation:

- symmetrical airfoil;
- camber effect neglected;
- including the effect of the angle of attack on a flat surface.

Indicating with Γ the circulation vortex and with r the perpendicular distance between the point and the line of the vortex, we have that in a two-dimensional field the speed induced for a vortex of infinite length will be:

$$V_\vartheta = \frac{\Gamma}{2\pi r} \tag{2.18}$$

The circulation has the same positive sign as its vorticity. Furthermore, it can be shown that in a three-dimensional field the induced velocity of a vortex element, of length dl and strength Γ, at a point P from a point Q is:

$$dV_p = \frac{\Gamma}{4\pi} \cdot \frac{dl \times r_{PQ}}{|r_{PQ}|^3} \tag{2.19}$$

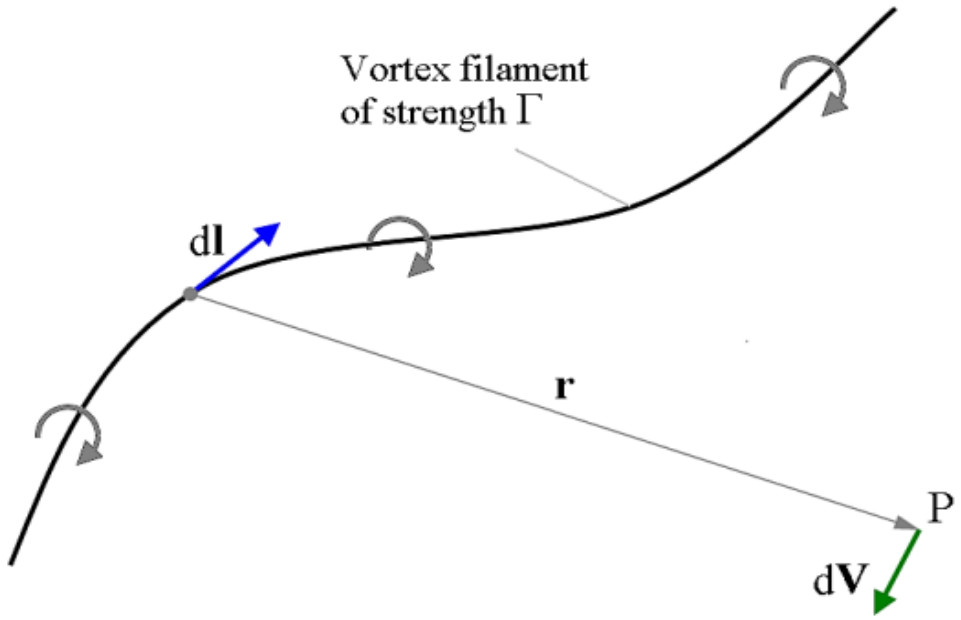

Figure 2.4: Vortex filament.

Equation (2.19) is also known as the Biot-Savart law and can be integrated over the length of the filament for the velocity induced at point P:

$$V_p = \frac{\Gamma}{4\pi} \int \frac{dl \times r_{PQ}}{|r_{PQ}|^3} \tag{2.20}$$

The main problem with the VLM is that it is not effective near the leading and trailing edges of the wing, where the thickness is very important. The problem with the method is the inability to calculate the local pressure distribution, whereas the values of the total and local forces appear to be quite reasonable. It should be noted that in OpenVSP the solver is not based on the classic VLM but is characterized by ring vortices distributed along the entire wing and only on the tail they extend to infinity [5].

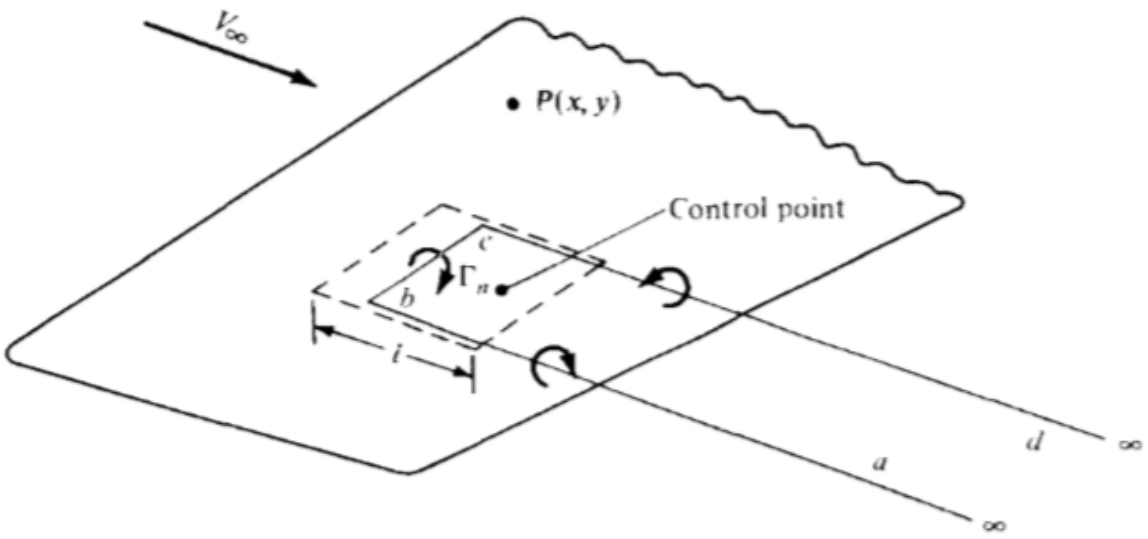

Figure 2.5: Horseshoe vortex scheme.

3. Modeling and Analysis Software

3.1 OpenVSP

OpenVSP also known as Open Vehicle Sketch Pad is a parametric geometry tool that allows the user to create a 3D model of an aircraft defined by common engineering parameters. OpenVSP's predecessors were developed by J.R. Gloudemans and others for NASA starting in the early 1990s. On January 10, 2012, OpenVSP was released as an open-source project under the NASA Open Source Agreement (NOSA) in version 1.3 [6]. OpenVSP displays a graphical user interface upon startup. The workspace is where the model is displayed while the geometry software lists the individual components in the workspace such as fuselage, wings or propellers. OpenVSP offers a multitude of basic geometries, common to aircraft modeling, that users modify and assemble to create models [7]. The setting of the values of U (spanwise) and W (chordwise) parameters for each component is crucial. This will make the analysis results more accurate.

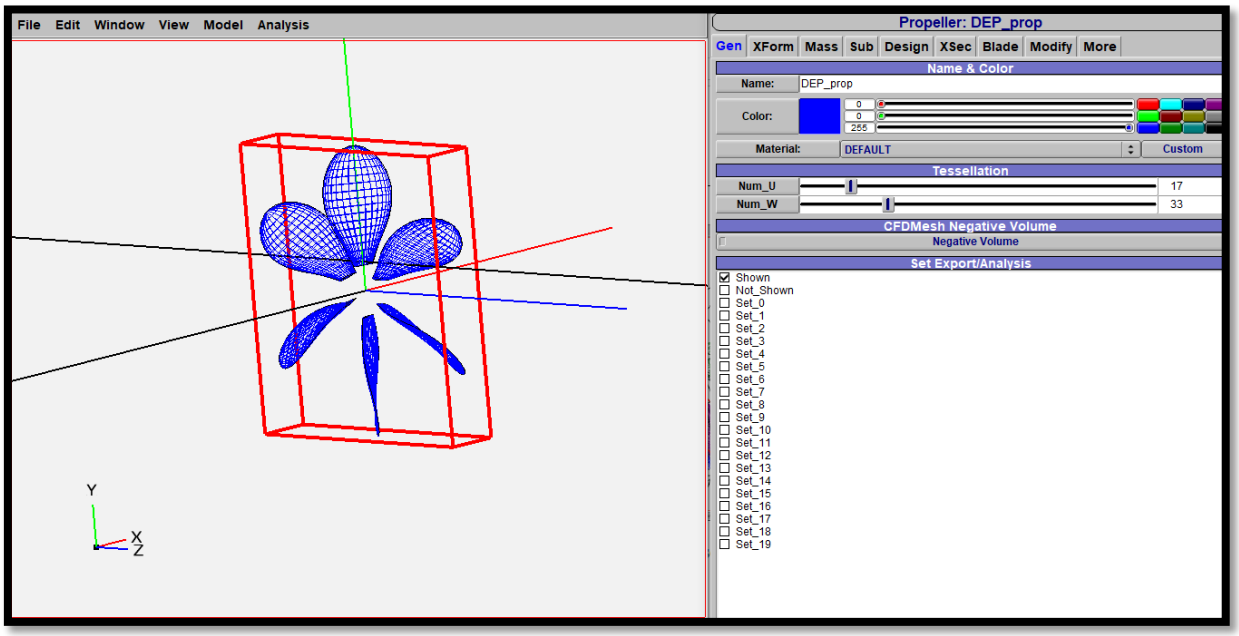

Figure 3.1: U e W setting for the geometry of the isolated DEP propeller.

3.2 VSPAERO

VSPAERO is a potential flow aerodynamics tool developed by Dave Kinney at NASA Ames. The solver was designed from the ground up to take advantage of OpenVSP geometries and the DegenGeom thin surface representation. In Figure 3.2 you can see how the data for the analysis was set up. By selecting Overview you can choose whether to use VLM or the panel method. You can also define the values for the flow conditions to be analyzed.

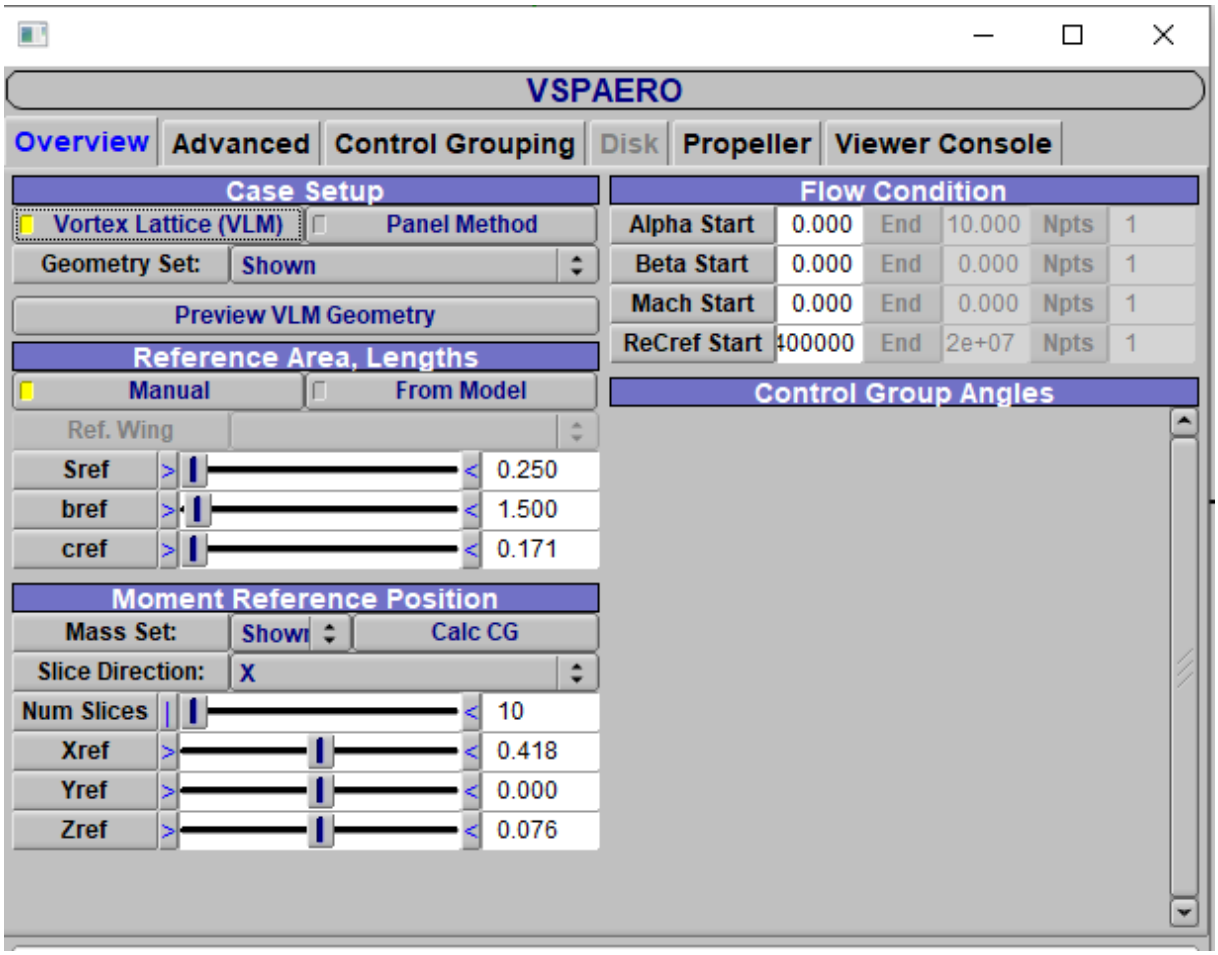

Figure 3.2: VSPAERO Overview.

VSPAERO also allows the analysis of propellers considering them as actuator disks or rotating propellers. Once all the values have been defined, you can click on Start solver to perform the analysis. All files containing the following information will appear in the OpenVSP folder:

- LOD file: contains the representation of the local lift coefficient, resistance and lateral forces;
- HISTORY file: contains the total integrated forces and moments;
- POLAR file: where the forces and moment coefficient are shown in a table as the input data changes [4].

Files can be opened with Excel or Notepad.

3.3 Geometric model of rotating propellers

The geometric model of the starting aircraft was obtained via OpenVSP from a previously done modeling to which the two different types of rotating propellers were added along the half-wings. In the following chapters we will see how this configuration was modified and the reason for this choice.

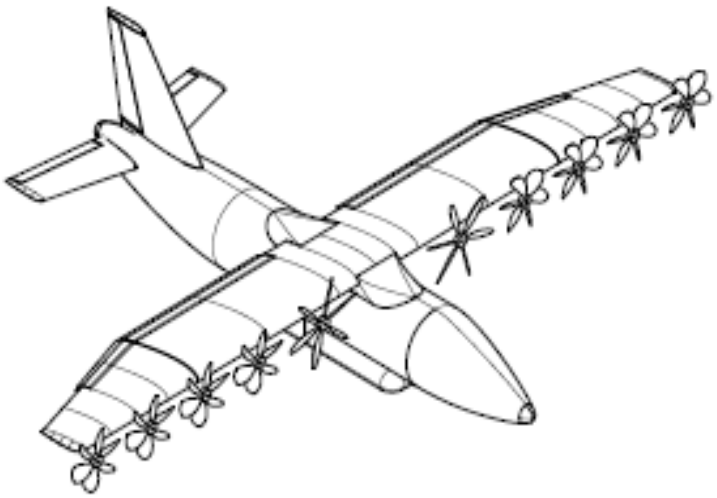

Figure 3.3: PROSIB 19-Pax model with propellers.

The rotating propellers added to the half-wings are of two types:

- THERMAL propellers, placed near the fuselage and coupled to thermal engines;
- DEP propellers, placed along the entire rest of the half-wing and coupled to electric motors.

The characteristics of the propellers are shown in the following tables:

DATA	VALUE	MEASURE UNIT
Number of blades	6	/
Disk Radius	0,0845	m
Hub Radius	0,01	m
Design Speed	20	m/s
RPM	8000	RPM
Thrust	3,5	Newton
Altitude	0	km
Design Lift Coefficient	0,7	/
CT	0,158	/
CP	0,328	/
J	1,55	/

Table 3.1: THERM propeller features.

DATA	VALUE	MEASURE UNIT
Number of blades	6	/
Disk Radius	0,0585	m
Hub Radius	0,01	m
Design Speed	20	m/s
RPM	10000	RPM
Thrust	4	Newton
Altitude	0	km
Design Lift Coefficient	0,7	/
CT	0,609	/
CP	1,383	/
J	1,03	/

Table 3.2: DEP propeller features.

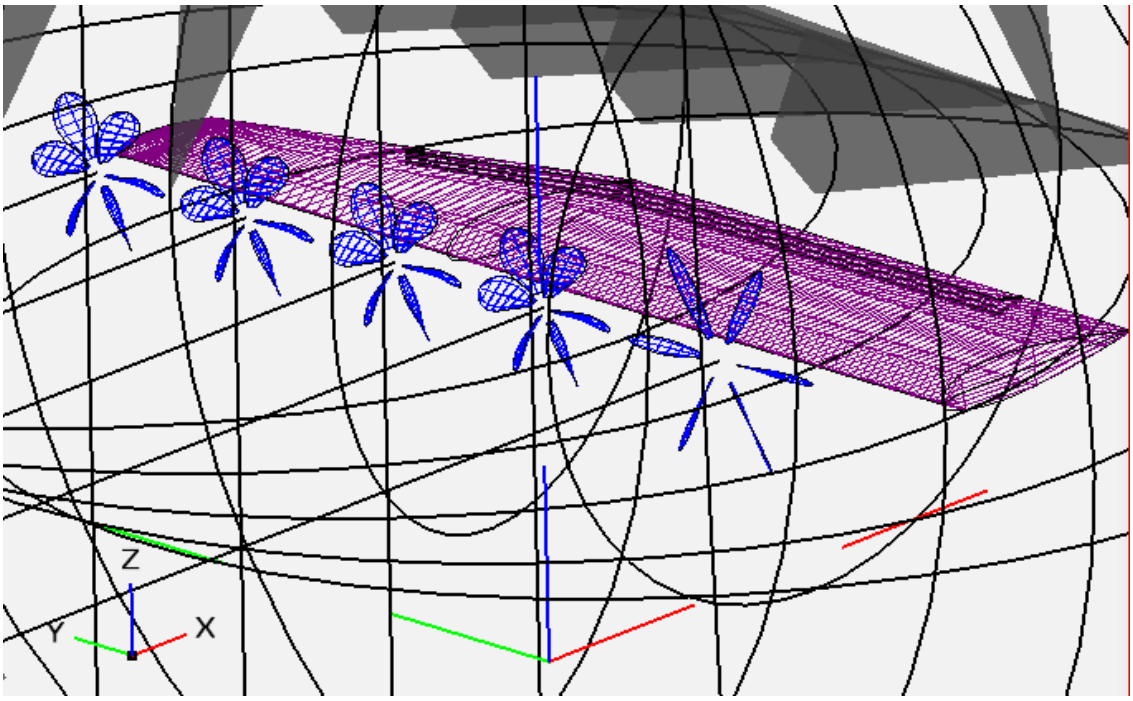

Figure 3.4: Propeller arrangement on the right half-wing.

It is here remarked that, while the aero-propulsive analysis discussed in [4] was performed with the actuator disk model in steady flow conditions, the current work focused on the implementation of the rotating blades model. Therefore, the propeller is discretized in a number of wings – with specific values of U and W refinements – equal to the number of blades. This set of blades rotates about the propeller axis, which defines a local reference system. VSPAERO then solves the unsteady flow field with a time-marching approach. Each time step starts from the solution of the previous one. It is good practice to start from a steady state solution and VSPAERO has an option to automatically do so.

Although established from the previous analyses [4], the propeller's coefficient CT and CP are calculated by VSPAERO as a result of the last revolution of the blades. The user has to set the RPM and the number of revolutions. It is crucial to set a number of revolutions and a number of wake nodes such that the propeller slipstream extends downstream until the region of interest (e.g. the aircraft tailplane). The time step can be automatically calculated by the solver, which defaults to a value such to achieve 15° of rotation per time step. The option to limit the far-field extension had no effect in the used OpenVSP version 3.39.1, differently as stated in Ref. [8].

For its own nature, the rotating propeller model needs an amount of computational time that is at least an order of magnitude bigger than the steady actuator disk. This is due to the

additional wing surfaces to be modelled as blades and the time marching approach, which requires hundreds of time steps to achieve the convergence to the desired number of propeller revolutions. If the actuator disk approach on a fit mesh model requires minutes to solve a polar, the rotating blades model requires hours just to analyze a single angle of attack.

To continue the analysis with VSPAERO it is necessary to add some input data which are shown in the table below:

INPUT DATA		
DATA	VALUE	M.U.
S_{ref}	0.250	m^2
b_{ref}	1500	m
c_{ref}	0.171	m
X_{ref}	0.418	m
Y_{ref}	0.000	m
Z_{ref}	0.076	m
AoA (start)	0.0	deg
AoA (end)	10.0	deg
Beta	0.0	deg
ρ_∞	1.225	kg/m^3
V_∞	20.0	m/s

Table 3.3: Input data VSPAERO.

4. Test Cases and Results

4.1 Isolated propeller

As anticipated in the previous chapter, following the coupling of the rotating propellers with the wing surfaces some convergence issues arose on the propeller wake. To try to solve these problems it was decided to isolate the DEP propeller and study its behavior. Some tests carried out have demonstrated how a careful choice of the computational grid, with cells denser in the chord direction and less dense in the span direction, led to sufficiently convergent results, reducing execution times. Furthermore, from an aerodynamic point of view, this led to obtaining a much more uniform wake compared to previous tests. To obtain the convergence of the propeller thrust and an acceptable wake form, the following values have been inserted: Num_U = 17; Num_W = 33; Wake nodes = 128; From Steady State and Uniform RPM options enables. See next figures.

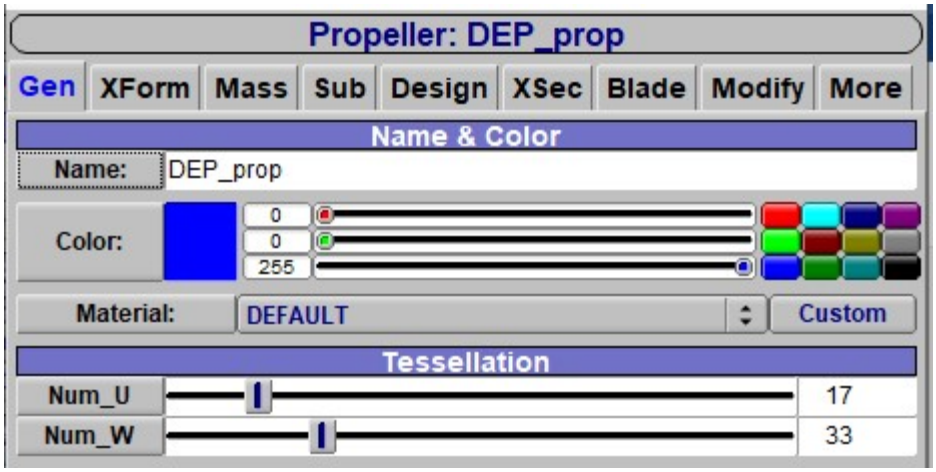

Figure 4.1: Computational grid DEP propeller.

Subsequently, by opening VSPAERO and clicking on Advanced it was possible to set the data as shown in figure 4.2.

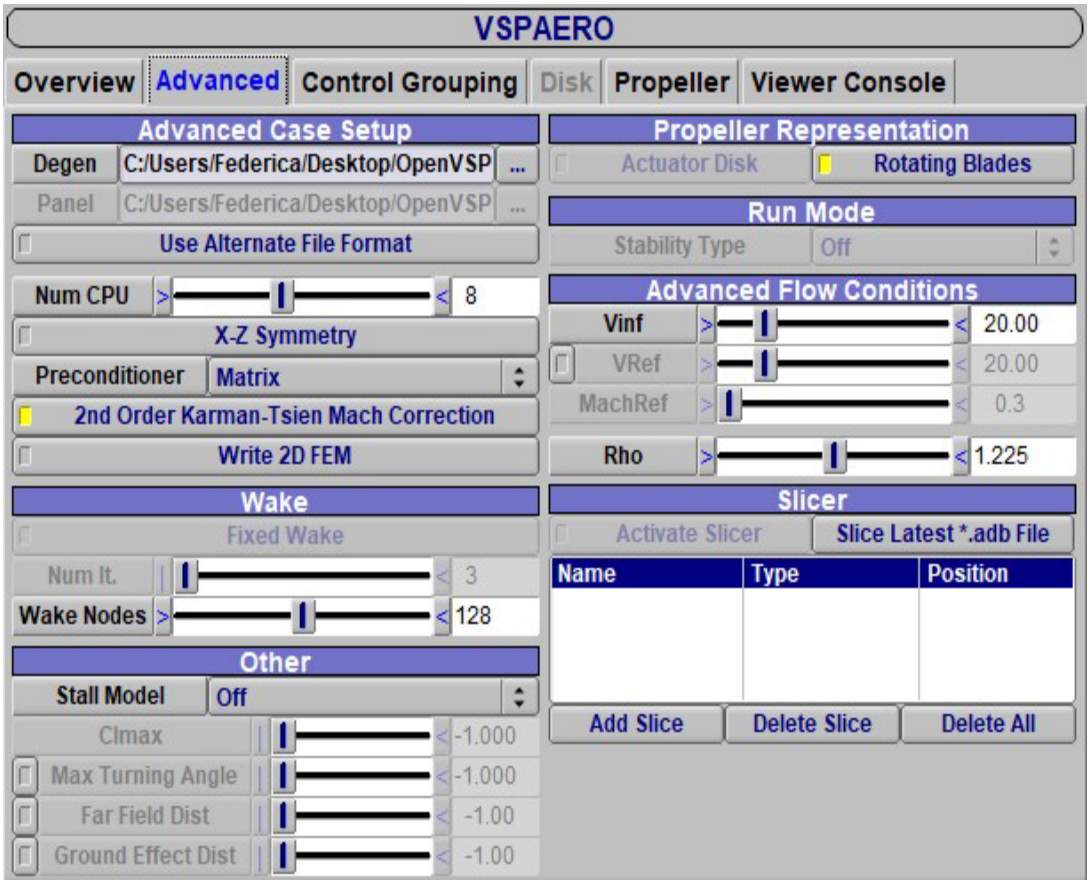

Figure 4.2: VSPAERO Advanced data setup.

When the propeller is modeled as a rotating blade in VSPAERO, specific inputs must be included as shown in figure 4.3.

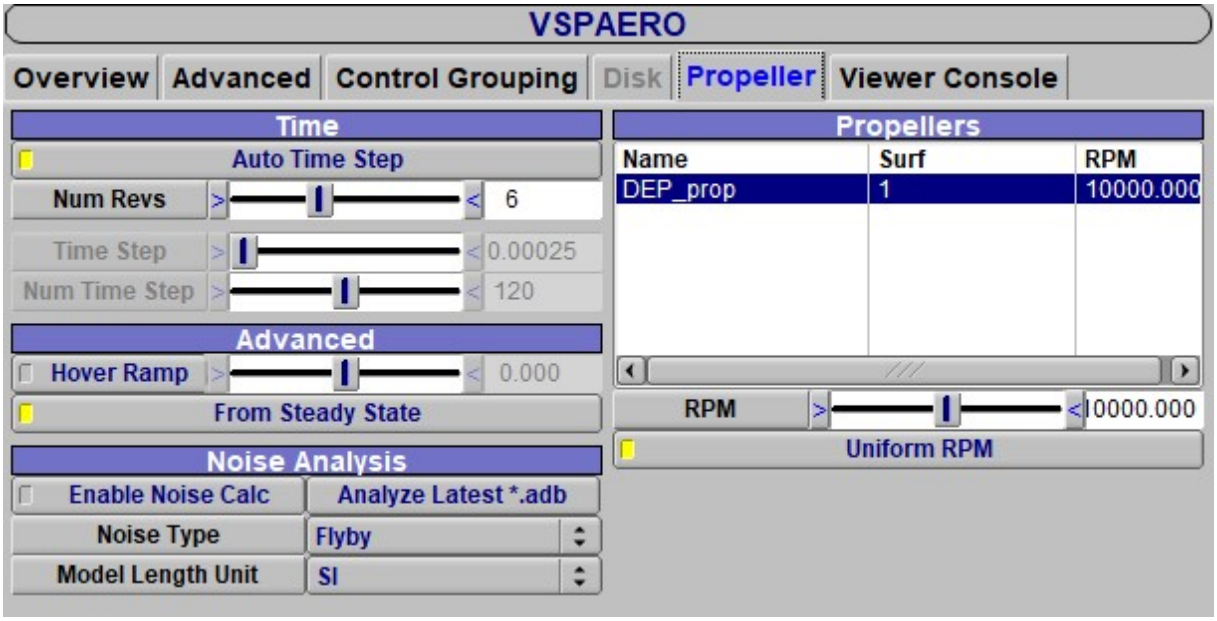

Figure 4.3: Propeller input setting.

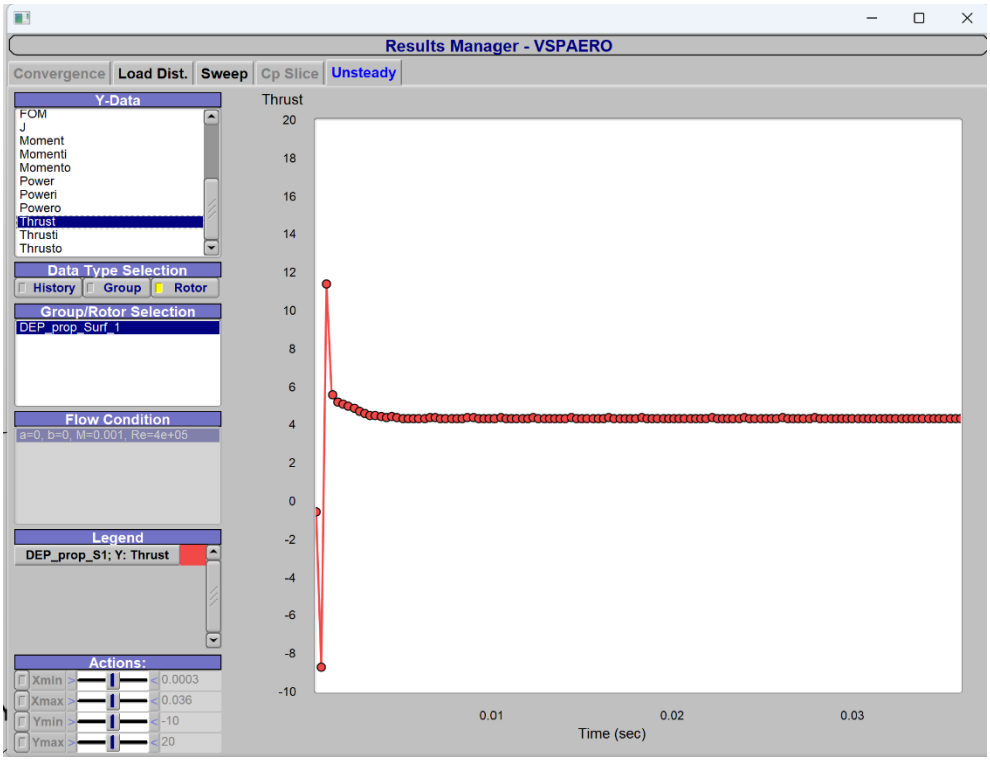

Figure 4.4: Isolated propeller thrust convergence.

At the end of the analysis, by clicking on Launch Viewer it is possible to see the shape that the wake of the propeller takes on.

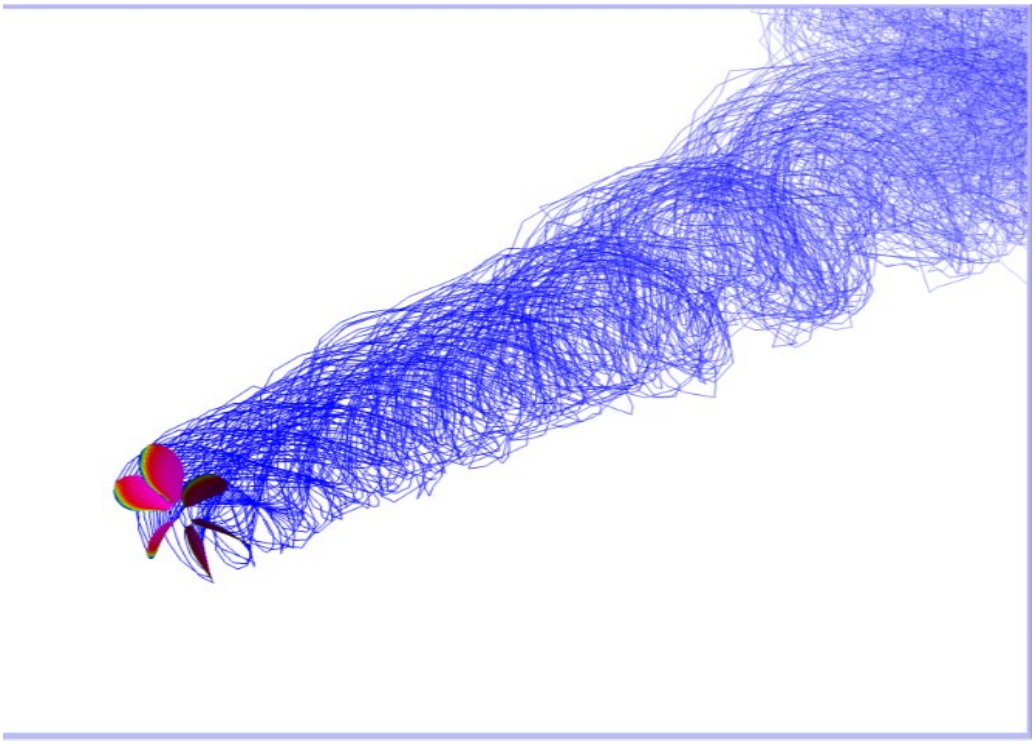

Figure 4.5: Isolated propeller wake trend.

4.2 Propeller- Wing- Plane

Once the behavior of the isolated propeller has been learned, it is possible to couple it to the wing and the horizontal tail plane to evaluate the effects on stability and in the aerodynamic field as the angle of attack (AoA) varies. Before proceeding with the comparison between the model with actuator disc and the model with rotating blades, a further comparison was made between the 12 revolution case and the 24 revolution case. The analysis has shown that after 24 revolutions the convergence does not improve compared to 12 revolutions, but rather the calculation times are doubled. For the case of our interest (wing-propeller-plane), we obtain calculation times of approximately 1h:40min for the 12 revolution case and 3h:30min for the 24 revolution case on a machine with an Intel i9-13900KF processor with 8 cores dedicated to VSPAERO. The figures below show the comparison between the two cases.

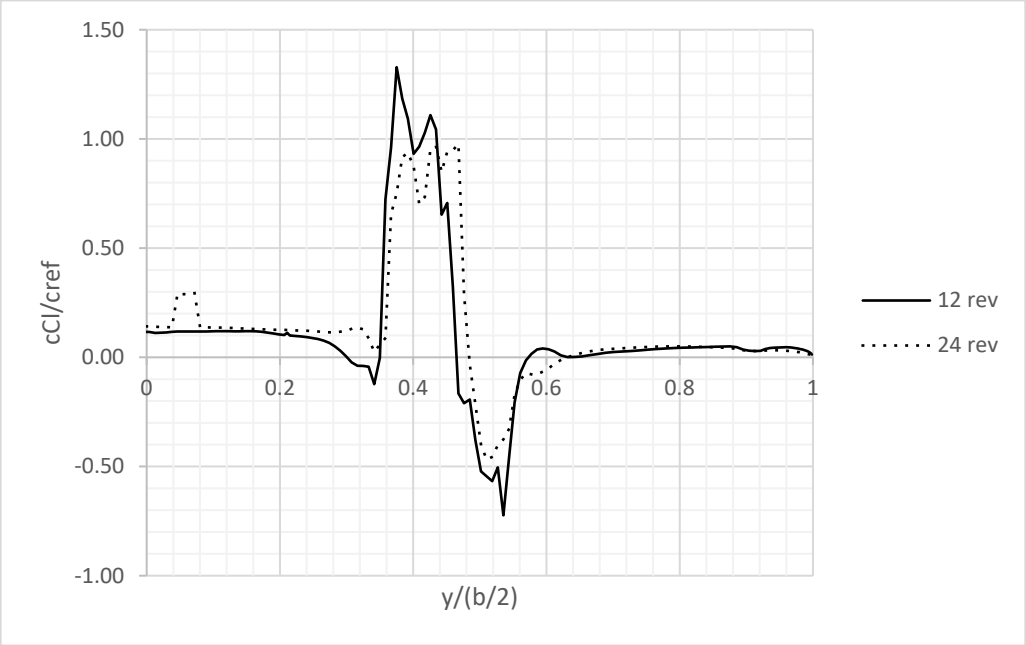

Figure 4.6: Comparison between 12rev. and 24 rev. wing span load distribution.

In Figure 4.6 you can see how the load along the wingspan in the case of 24 rev. does not appear to have improved compared to the 12 rev case.

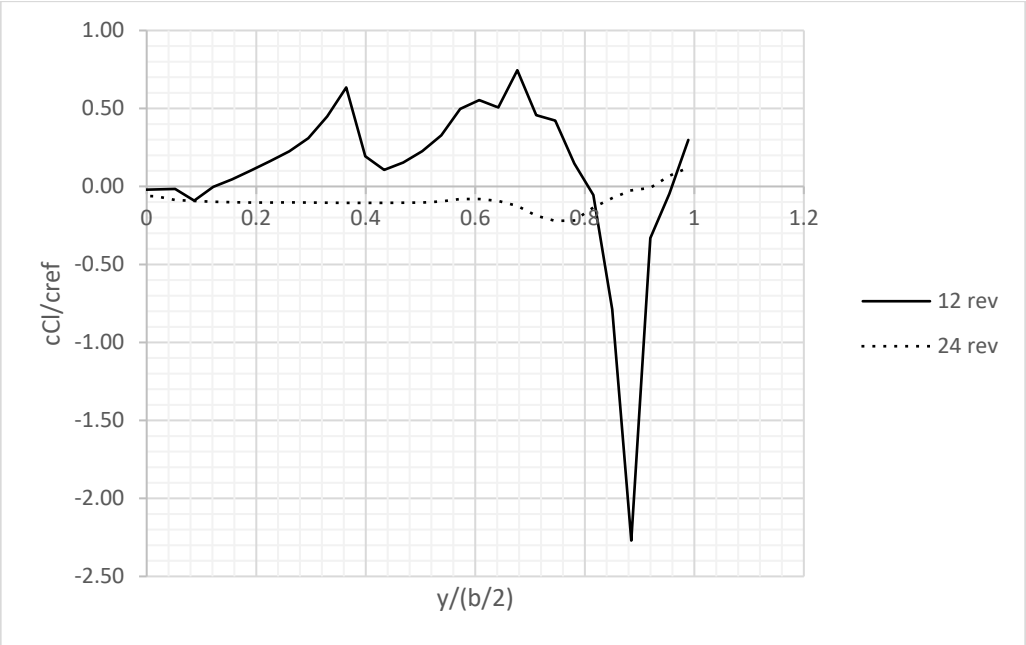

Figure 4.7: Comparison between 12rev. and 24 rev. tail plane span load distribution.

From Figure 4.7 you can see how the load on the tail plane is more realistic in the 24 rev case. compared to the 12 rev case.

Furthermore, to have a comparison between the behavior of the rotating blades and the actuator disk, the analyses were repeated with VSPAERO by setting the data on Actuator Disk. The results obtained were plotted on Excel and compared with those obtained from the analyses with rotating blades. In the following graph it is possible to see the distribution of loads along the wingspan both in the case of rotating blades and in the case of actuator disk for angle of attack $\alpha = 0°$.

From Figure 4.8 it can be observed that the wing loading – defined as the product of the local chord by the local lift coefficient and normalized by the reference chord – is smoother with the actuator disk method.

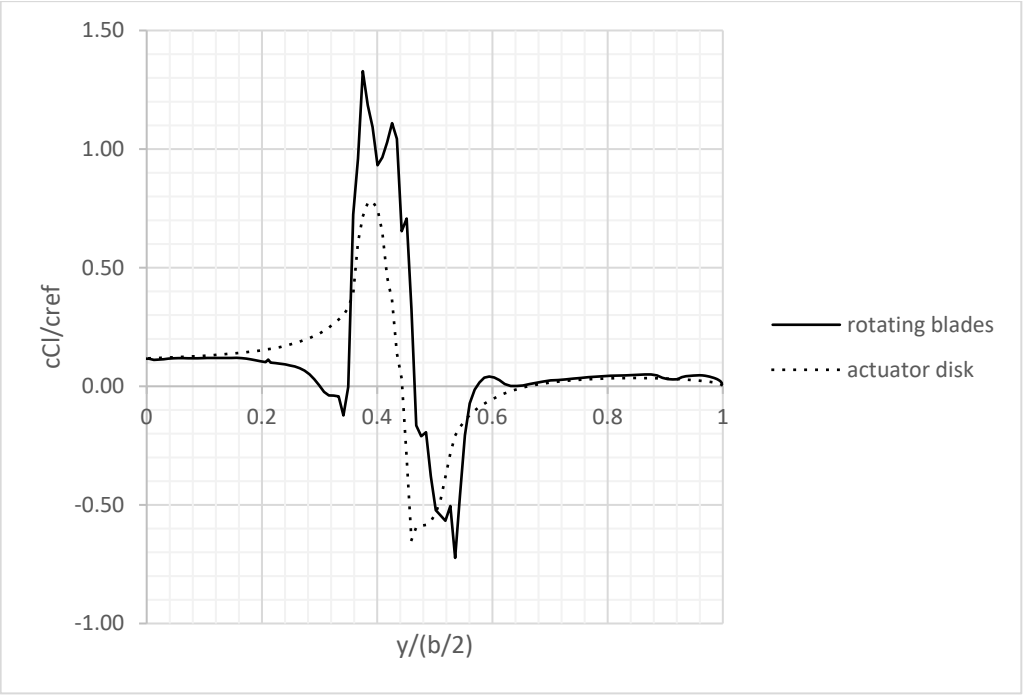

Figure 4.8: Comparison of wing span load distribution α=0°.

Similarly, the distribution along the span of the horizontal tailplane is shown in Figure 4.9. The tailplane load is strongly influenced by the propeller wake (see Figure 4.10) with both upwash and downwash regions. The achieved values are unreasonably large, especially if compared to those of the wing. This behavior can be attributed to convergence issues or to the limit of vortex lattice methods in computing wakes interacting with surfaces and other wakes.

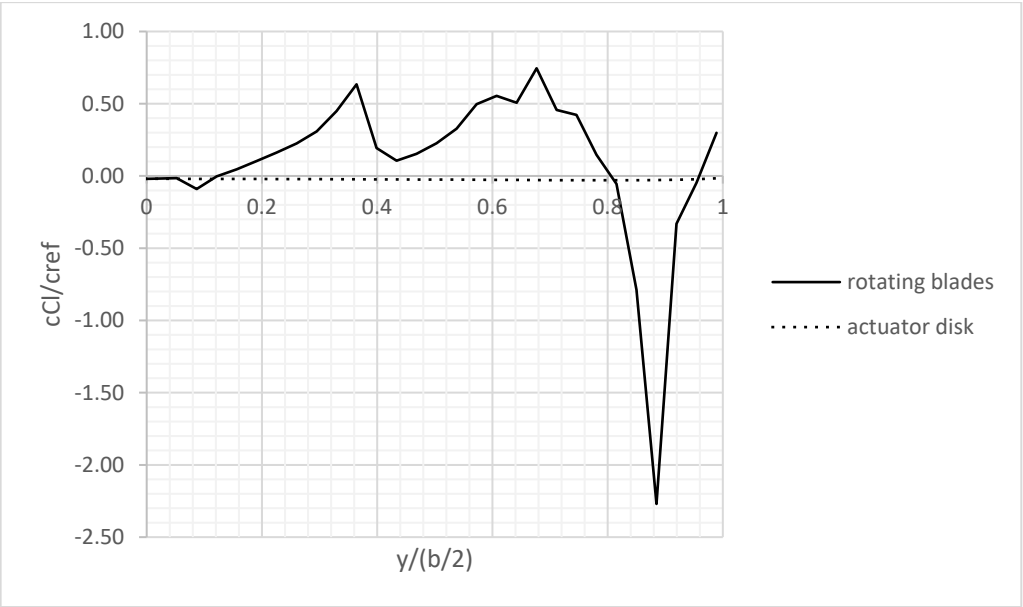

Figure 4.9: Comparison of loads along the tail plane span at α=0°.

In Figure 4.10 it is possible to see how the propeller wake interacts with the wing and tailplane wake at α=0°. Just downstream of the wing, the propeller wake becomes unusually large, affecting the tailplane load and wake. Far downstream the shape of the wake is unrealistic.

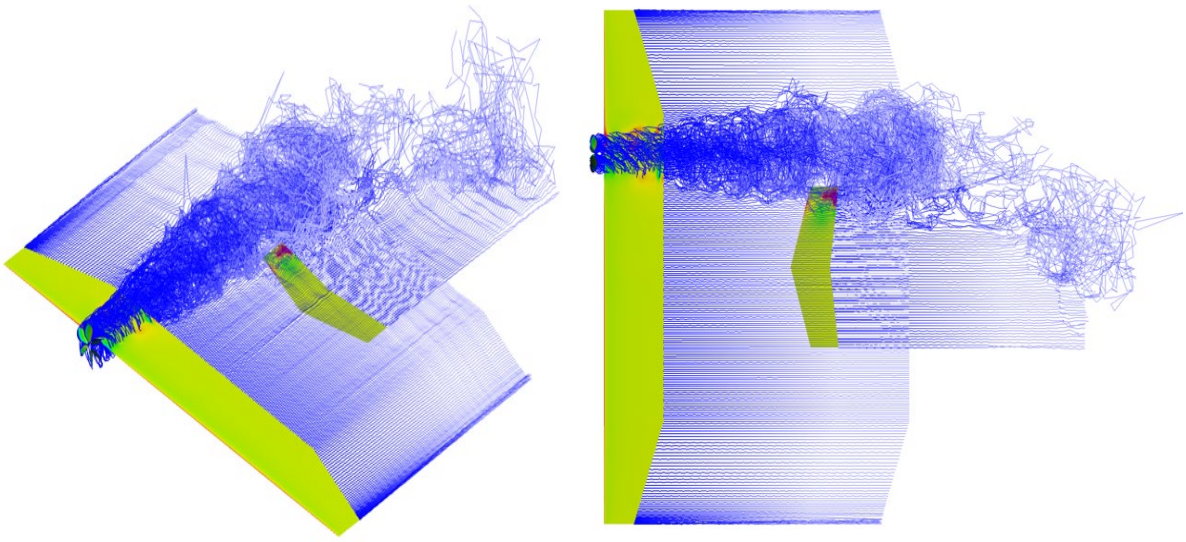

Figure 4.10: Propeller-wing-plan wake trend, α=0°.

From Figure 4.11 it can be observed, as in the previous case, that the wing loading is smoother with the actuator disk method. Also, the wing loading due to the rotating blades is smaller than that calculated with the actuator disk.

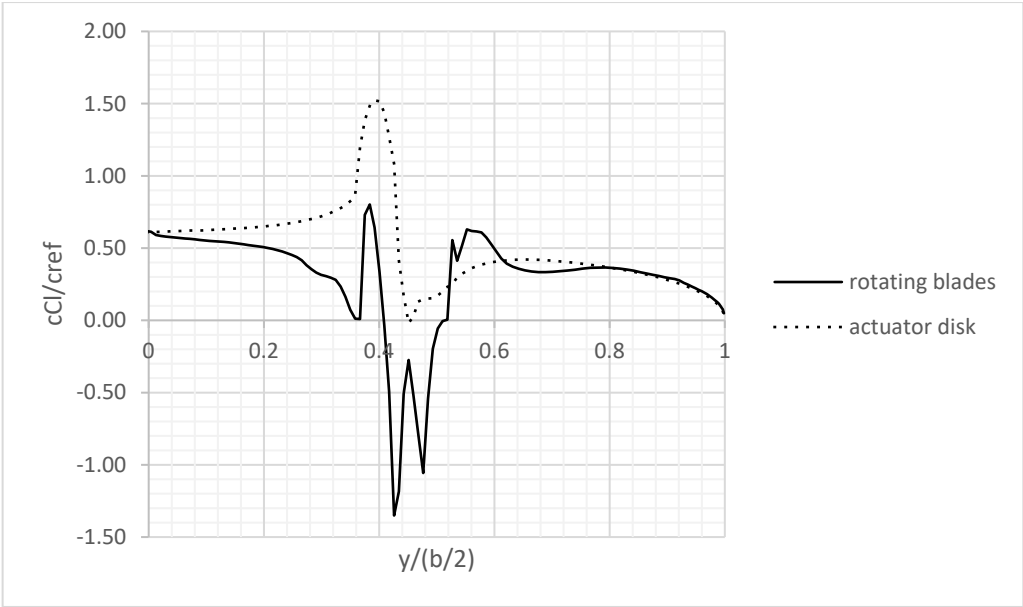

Figure 4.11: Comparison of wing span load distribution α=5°.

Similarly, the distribution along the horizontal tailplane is shown in Figure 4.12. The tailplane load is influenced by the propeller wake at its tip. With respect to the previous case at zero angle of attack, the horizontal tailplane aerodynamic load calculated with the rotating blades is close to that evaluated with the actuator disk method up to 80% of tailplane span.

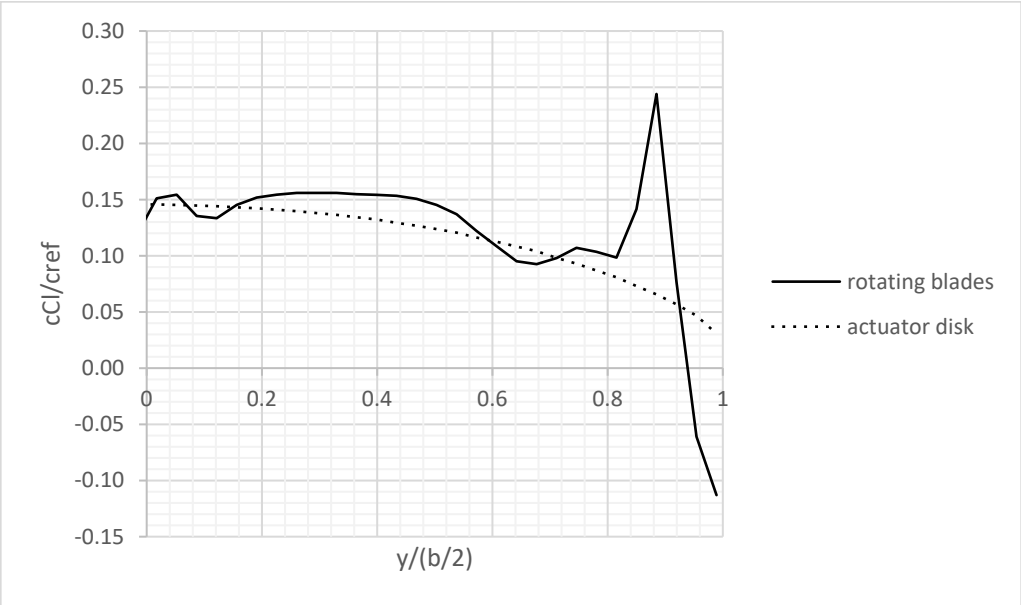

Figure 4.12: Comparison of loads along the tail plane span α=5°.

In Figure 4.13 it is possible to see the wakes interaction on the wing-tail combination with propeller at α=5°. Again, the shape of the wake becomes unrealistic far downstream.

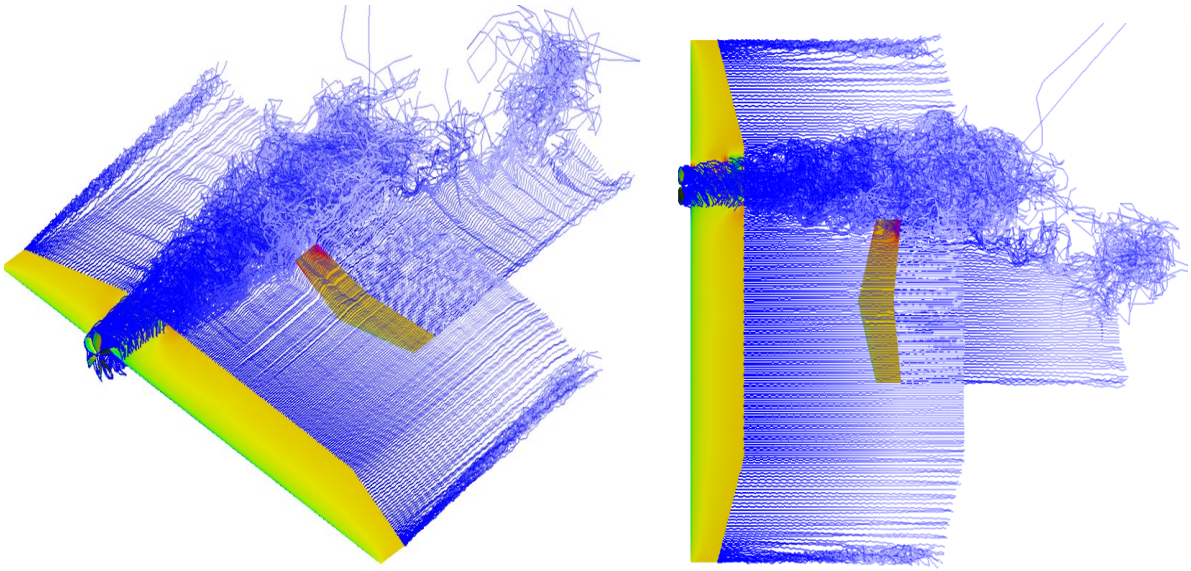

Figure 4.13: Propeller-wing-plan wake trend, α=5°.

From Figure 4.14 it is possible to see how even in this last case the wing loading curve is undoubtedly smoother with the actuator disk method at α=10°. Rotating blades provides a significantly larger wing load.

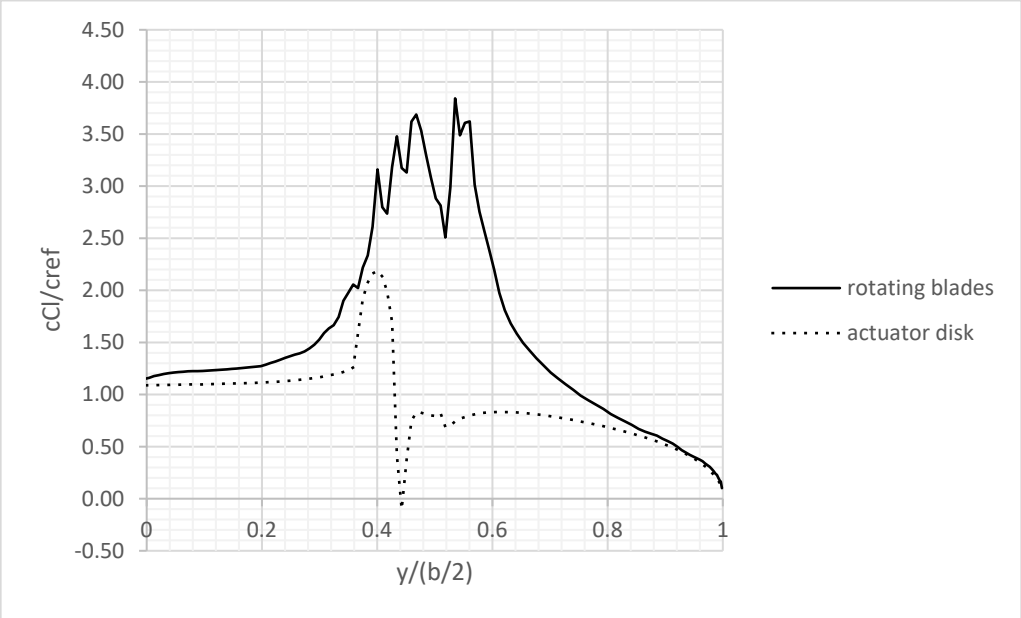

Figure 4.14: Comparison of wing span load distribution α=10°.

In Figure 4.15 it can be seen how the load along the horizontal tail span is strongly influenced by propeller wake with a large upwash region at about 80% tail span. Since the wing and propeller wakes are more distant from the tailplane at α=10°, the tailplane aerodynamic loading is smooth even with the rotating blades.

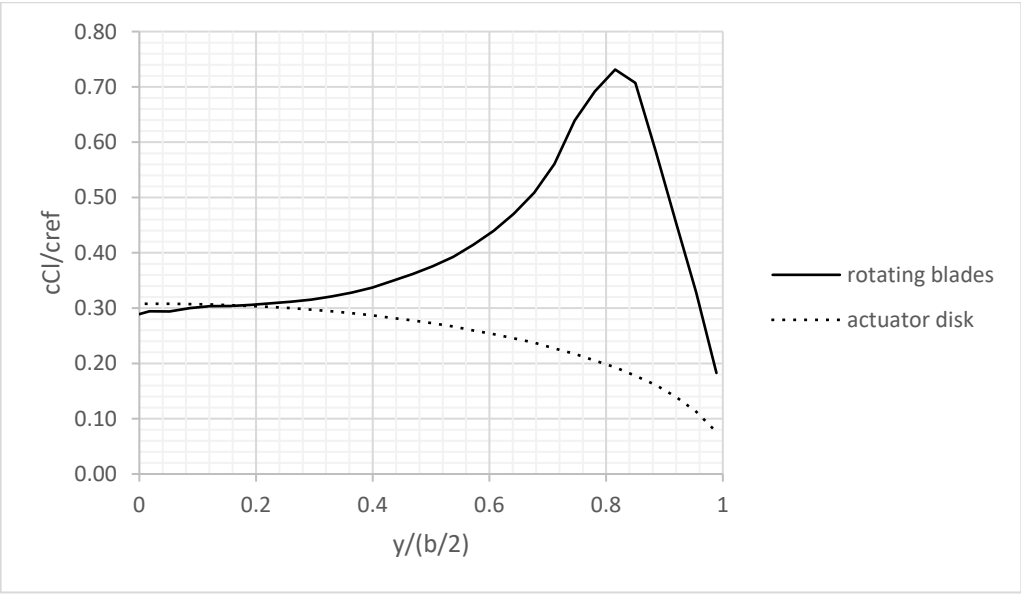

Figure 4.15: Comparison of loads along the tail plane span α=10°.

Finally, in Figure 4.16 you can see how the tail plane and the wing are influenced by the wake of the propeller.

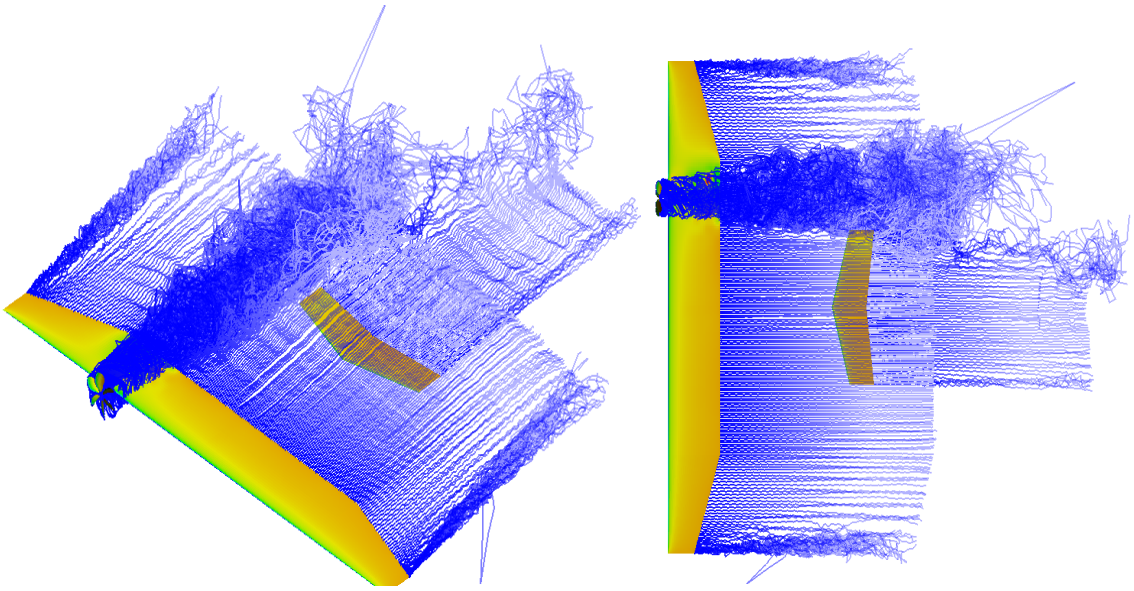

Figure 4.16: Propeller-wing-plan wake trend, α=10°.

From the obtained results it is possible to generate the polar graphs obtained by plotting the global coefficients with the different attack angles both in the case of actuator disk and in the case of rotating blades. In the following graph you can see how the CL lift coefficient curves are almost superimposed, both for the actuator disk and for the rotating blades in the section that goes at α = 0° and α = 5° and then you can notice a higher slope of the CL curve for the rotating blades compared to the actuator disk. This effect is not expected to happen in reality.

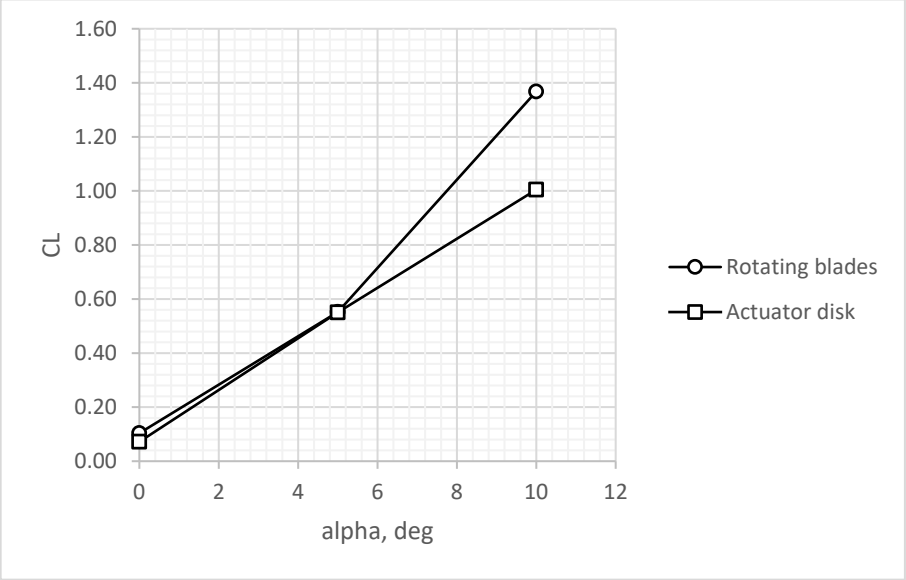

Figure 4.17: CL vs. α comparison curve.

Furthermore, as can be seen from the graph in figure 4.18, the CM coefficient curves have a different behaviour, in the case of rotating blades the curve follows a slightly negative trend and then increases positively, while in the case of actuator disk the curve has a slightly negative trend positive and then increases negatively. The last curve is undoubtedly wrong, since the aircraft is longitudinally stable [4]. This is another indication on how the rotating blades approach in VSPAERO, despite the initial successful tests, can hardly provide acceptable results, at least for the configuration investigated with the available computational resources.

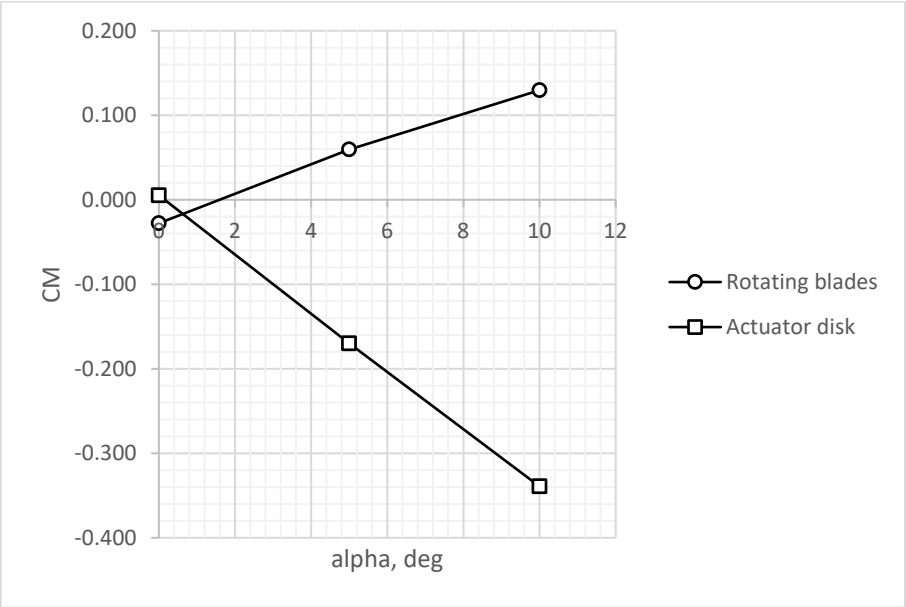

Figure 4.18: CM vs. α comparison curve.

In figures 4.19 and 4.20 the curves of the drag polar and aerodynamic efficiency (lift-to-drag ratio) are plotted and compared between rotating blades and actuator disk. The actual drag provided by VSPAERO is the vortex-induced contribution with a small, but insufficient, correction for profile drag. Therefore, CD is much more close to the induced drag coefficient than to the total drag coefficient.

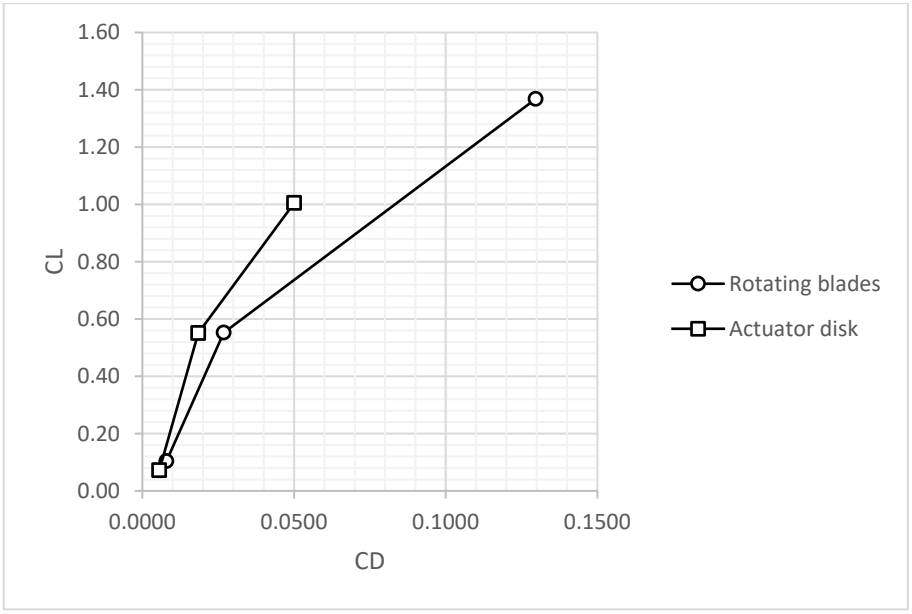

Figure 4.19: CL vs. CD comparison curve.

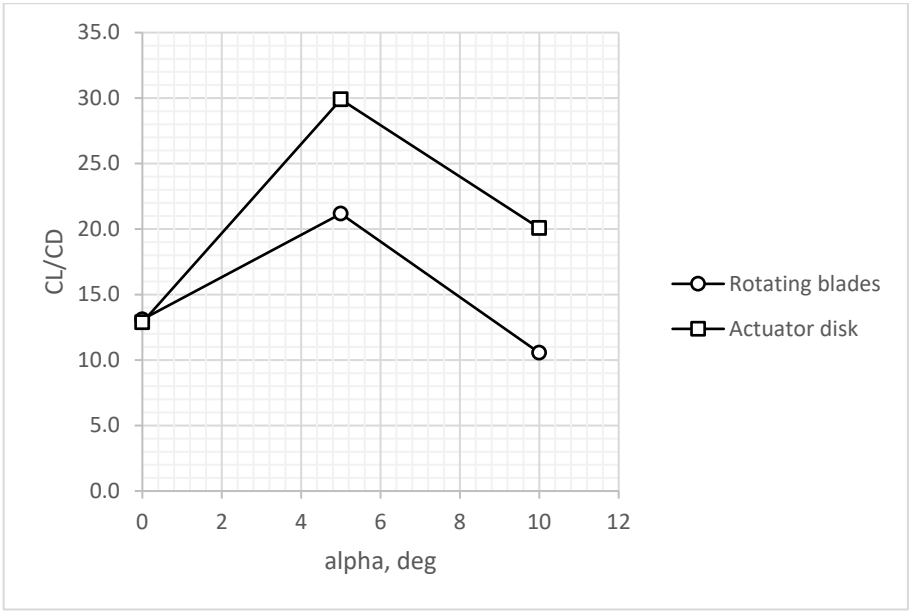

Figure 4.20: CL/CD vs. α comparison curve.

5. Conclusion

Concluding this thesis it is clear to note that the use of VSPAERO is extremely advantageous for aircraft design. Especially in the early design stages, VSPAERO provides valid insights into the aerodynamic characteristics of the project. This approach allows you to speed up, simplify and avoid wasting resources during the design process. However, it is possible to note some limitations of VSPAERO, in fact it is known that these methods have difficulty in capturing the aerodynamics of contrails impacting another body. Furthermore, as has been shown, it is not worth taking so much time for the setup and for the calculation of the propulsive effects with the rotating propeller model, in fact if this converges well, it leads to results very similar to those of the actuator disk. Recent studies have shown that the execution times of the wing with propeller modeled as an actuator disk in VSPAERO with VLM are on average between 4 and 8 minutes; while for the wing with propeller modeled as rotating blades in VSPAERO with VLM, execution times on average are approximately 370 minutes per angle of attack on an average laptop computer. Despite its limitations VSPAERO can be valuable during the conceptual and early design phases where quickly acquiring the approximate solution is of greater importance than obtaining an accurate analytical solution. Further studies are recommended to investigate the broader applicability of VSPAERO in modeling a variety of other propeller-wing-plane interactions and/or flight conditions.

Bibliography

[1] Nicholas K Borer et al. “Design and Performance of the NASA SCEPTOR Distributed Electric Propulsion Flight Demonstrator”.

[2] Hydun D Kim, Aaron T Perry, and Phillip J Ansell. “A Review of Distributed Electric Propulsion Concept for Air Vehicle Technology”.

[3] Nicholas K Borer et al. “Comparison of Aero-Propulsion Performance Predictions for Distributed Propulsion Configurations”.

[4] Marchetti Giulia. “Effects of the distributed propulsion on the stability and control characteristics of a 19-Pax aircraft model”.

[5] Ambrosino - Di Martino. “Aerodynamic analysis and surrogate modelling of distributed propulsion on commuter and regional aircraft through VLM and CDF methods. 2018/2019.

[6] OpenVSP. URL: https://openvsp.org/learn.shtml.

[7] OpenVSP. URL: https://en.wikipedia.org/wiki/OpenVSP.

[8] Carla N D Sheridan, Dahlia D V Pham, and Siena K S Whiteside. “Evaluation of VSPAERO Analysis Capabilities for Conceptual Design of Aircraft with Propeller-Blown Wings”.